

FULL PAPER

Enhanced Stability and Conductivity of (polyaniline-chitosan) Composites

Fernando Ratuchne*, Marins Danczuk, and Eryza Guimarães de Castro

Departamento de Química, UNICENTRO, Rua Simeão Varela de Sá, 03, Guarapuava, 85040-080, Brasil

Article history: Received: 27 October 2017; revised: 05 January 2018; accepted: 10 January 2018. Available online: 21 May 2018. DOI: <http://dx.doi.org/10.17807/orbital.v10i3.1110>

Abstract:

This study describes the synthesis of Pani-Chitosan soluble hybrid composite through an *in situ* polymerization of aniline in hydrochloride acid media in the presence of chitosan. The optical, morphological, structural, thermal and electrochemical characteristics of these materials were studied by UV-Vis, FTIR, SEM, TG and CV analysis. From UV-Vis and FTIR, the formation of composite was confirmed. The SEM images show that Pani presented agglomerate morphology, while Pani-Chitosan composite shows plate-like morphology, with higher surface area and the TG results showed that Pani-Chitosan has greater thermal stability. The electrochemical measurements indicate that Pani-Chitosan material presents upper current density at all scan rates studied, sharper and shifted peaks to more negative potentials, indicating that the charge injection processes are easier. These results indicate that the composite material is promising for application in electrochromic devices and capacitors, because of its greater surface area, thermal and electrochemical stability.

Keywords: biopolymer; capacitor; composite; conducting polymers

1. Introduction

Intrinsically conductive polymers have been continuously studied since the discovery of the conductivity of polyacetylene in 1977 [1]. They are insulators or semiconductors in their pure form, but have their conductivity increased several orders of magnitude when doped [2]. Polyaniline (Pani) had its electrical properties discovered in the 80's, highlighting among the conductive polymers [2]. Its use is mainly due to easy synthesis and doping/dedoping process, low production cost, high reliability, multiple oxidation states, high theoretical capacitance (2000 Fg^{-1}), high conductivity when doped, environmental stability, electrochemical, optical and electronic properties. On the other hand, the difficulties in its use are attributed to the poor electrochemical life cycle due to the alteration of volume and structure during the process of insertion/disintegration of the counter ions, their processability and low mechanical, thermal and electrochemical resistance. Several research groups looking forward to improve the Pani properties by

synthesizing composites/hybrids materials with biopolymers, searching for the synergism between the properties of Pani (conductivity) and biopolymer (solubility, mechanical strength and electrochemistry) [3, 4].

Pani and its composites have been applied as a sensor for Hg (II) [5], volatile basic nitrogen molecules [6, 7], aliphatic amines [8], acetone [9], toluene, triethylamine [10], pheromone 2-heptanone [11], estradiol, humidity [12], corrosion protection [13], electro-reduction of CO_2 [14], membrane for the ion separation [15], removal Cu (II) in water [16], capacitors [17–21], battery [22–24], fuel cells [25], optical [26], electroanalytic [27], photoelectrochemical [28] and photocatalytic [29] applications. The chitosan is having $-\text{NH}_2$ and $-\text{OH}$ groups, which offers self-doping, one of the chemical advantages to interact with Pani, and enhances its properties.

Chitosan is a natural cationic polyaminosaccharide, obtained from the complete or partial deacetylation of chitin. This biopolymer has high hydrophilicity, important biological

*Corresponding author. E-mail: fratuchne@hotmail.com

properties, biodegradability, biocompatibility and bioactivity[4], non-toxic, low cost [30], ability to form films, chemical inertia, high mechanical strength, antibacterial properties [31]. Its direct application is restricted by some factors, the most relevant is the low electrical conductivity and response time. In order to overcome these constraints, composites have been prepared by incorporating a rigid polymer network (conductive polymers) into the flexible polymer matrix (chitosan), combining good processability of chitosan with the electrical conductivity of conducting polymers [32].

There are many studies regarding the use of Pani-chitosan materials as a sensor and in adsorption applications, but the majority of the studies describes the use of crosslinking agent and do not use *in situ* polymerization[31, 33–35]. Moreover, there is not a discussion about the capacitive behavior of the Pani-chitosan materials. The scope of this study was to develop simple, cost-effective, and environmental friendly synthesis of Pani-Chitosan hybrid via synthesis *in situ*. The proportion of chitosan was studied and structural, morphological and electronic

characterization of the materials was discussed.

2. Material and Methods

2.1 Sample Preparation

The experimental procedure was adapted from the literature [36, 37] and is shown in Figure 1. Aniline was solubilized in HCl solution (1.0 mol L^{-1}), followed by the dropwise addition in the chitosan solution (6.25 , 12.5 and 25 g L^{-1}) in 4% acetic acid solution, under stirring during 20 min. The solution of oxidizing agent $(\text{NH}_4)_2\text{S}_2\text{O}_8$ (0.14 mol L^{-1}) was added dropwise under stirring. This system was kept under stirring during 24 h, at room temperature. The final solution was centrifuged and the precipitate was washed several times with HCl solution (0.1 mol L^{-1}), ultrapure water and dried at $50 \text{ }^\circ\text{C}$.

The materials prepared with higher concentrations of chitosan had phase separation during the drying process. Because of this, they were discarded and only the material prepared with 6.25 g L^{-1} has been studied.

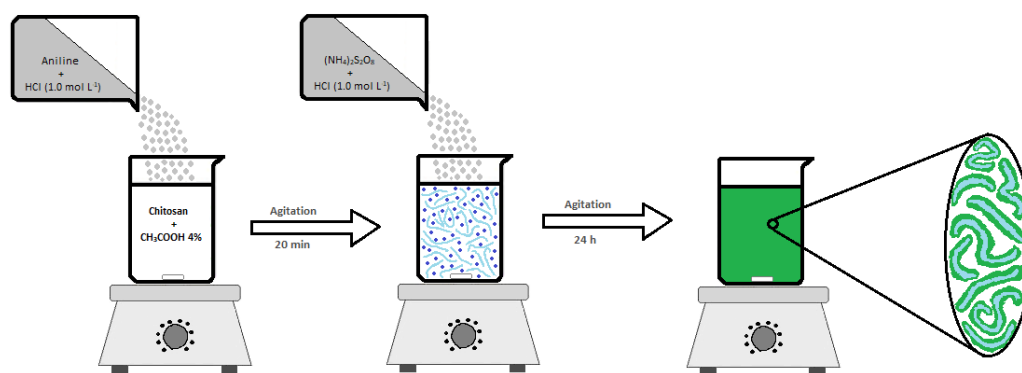


Figure 1. Schematic representation of the synthetic method used to obtain the Pani-chitosan composite.

2.2 Characterization techniques

Ultraviolet-Visible experiments were done on a UV-Vis, UV-1800 Shimadzu spectrophotometer, using a quartz cuvette and N-methyl-2-pyrrolidone as the reference (Pani is not soluble in aqueous electrolytes), in the 300-1000 nm range. Infrared spectra (FTIR, Vertex 70, Bruker) were obtained using the attenuated reflectance technique (ATR) on zinc selenide crystals, with

resolution of 4 cm^{-1} and 400 to 3500 cm^{-1} range. Morphology studies of polyaniline samples were carried out on a Scanning Electron Spectroscopy (VEGA3 TESCAN) operating with secondary electron. Thermal analysis (SDT Q600) measurements were performed by Thermogravimetric Analysis (TG) in the range from 20 to $800 \text{ }^\circ\text{C}$, with a heating ramp of $10 \text{ }^\circ\text{C min}^{-1}$, under N_2 atmosphere. The electrochemical

characteristics of the materials were evaluated by cyclic voltammetry using a μ -autolab potentiostat, Type III (Metrohm) and Nova software (version 1.10). The voltammograms were performed H_2SO_4 (0.5 mol L^{-1}) as electrolyte, in a conventional three electrodes cell, which consist of working electrode, a platinum plate as counter electrode and Ag/AgCl (3 mol L^{-1}) as reference electrode. We had chosen paste electrodes as the working electrode because the Pani-Chitosan material is soluble in the aqueous electrolytes. This working electrode was constructed using graphite, the active material (Pani or Pani-Chitosan) and 25% w/w of mineral oil as a binder, is related as the best proportion. The mixture was ground thoroughly in an agate mortar with a pestle for 20 min, and a homogeneous paste was obtained. It was studied the better proportion of active material (not shown) varying from 5 to 100%, and the best results were obtained with 10% of active material providing in the paste. The modified paste was placed firmly into a plastic syringe (0.0314 cm^2) with a copper wire as the conductor. To ensure an active and fresh surface, the electrodes were manually abraded gently on a sheet of paper between the experiments.

3. Results and Discussion

Figure 2 shows the UV-Vis spectra of Pani and Pani-Chitosan samples in N-methyl-2-pyrrolidone. The UV-Vis spectra show the characteristic bands of Pani in the emeraldine salt form. The absorption band in 365 only appears at high levels of doping, because it comes from a combination of 360 e 440 nm bands, assigned to π - π^* transition of benzenoid segment and polaron- π transition in quinoid rings, respectively. The band at 900 nm is relative to π -polaron transition [37, 38]. Furthermore, the π -polaron band has a displacement of 900 to 793 nm in Pani-Chitosan and it has a broad electronic transition "tail", it indicates the free-carrier absorption and extended chain conformation. These results is a good indicative of the interaction of Pani and chitosan chains [37].

Figure 3 shows the ATR-FTIR spectra of the Pani and Pani-Chitosan samples. These spectra present the characteristics bands of emeraldine salt: 1100 cm^{-1} , assigned to $\nu(\text{C-N}^+=\text{C})$ stretching [17, 21, 39] and 1225 cm^{-1} , due to cation radical

$\nu(\text{C-N}^+)$ stretching [17]. The bands in 1438 [17, 21] and 1550 cm^{-1} [17, 21, 39] are assigned to stretching in benzene and quinoid rings, respectively, and are also used to estimate the oxidation degree of the polymer. The band at 1664 cm^{-1} is assigned to $\nu(\text{C-C})$ stretching in benzene ring [40]. The shoulder, observed in 1580 cm^{-1} , is assigned to polaronic $\nu(\text{C}=\text{C})$ stretching, active in the infrared only by means of alteration of symmetry, promoted by a conformational change of the Pani chains. Some of the bands are attributed to stretching of both Pani and chitosan, and confirm the formation of the composite: 783 and 3215 cm^{-1} are assigned to $\nu(\text{N-H})$ stretching [39, 41] and 1281 cm^{-1} stretching from $\nu(\text{C-N})$ [40–42]. The suppression of the other characteristics bands of chitosan is an indicative of the presence of Pani chains in the polymer network of chitosan. The band at 1016 cm^{-1} is assigned to $\nu(\text{C-O-C})$ stretching vibrational modes [43]. The new band at 3030 cm^{-1} can be assigned to stretch of new bond formed between Pani and Chitosan chains.

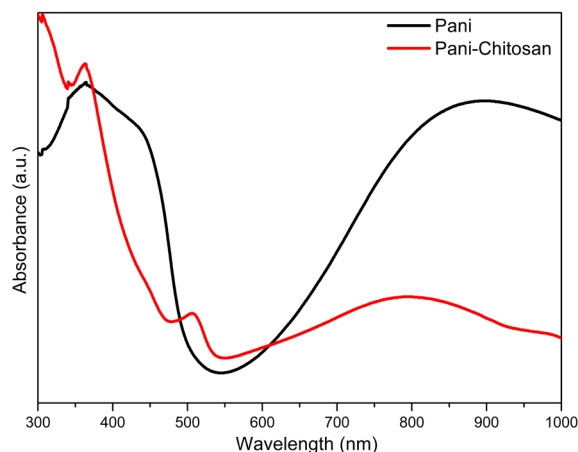


Figure 2. UV-Vis spectra of material in N-methyl-2-pyrrolidone.

Figure 4 shows the SEM images of Pani and Pani-Chitosan in different magnifications. Pure Pani presented undefined morphology in the form of agglomerates (Figure 4a, c and e). However, Pani-Chitosan showed a plate-like morphology, as can be seen in Figure 4b, d and f. This data suggests that the polymerization of the aniline occurred on the surface of chitosan chains, with chitosan acting as a template.

The morphological characteristics of the Pani-Chitosan composite indicate higher organization

of Pani chains in this material, in other words, more linear chains, as also suggested by UV-Vis spectra. Therefore, Pani-Chitosan should exhibit higher conductivity due to upper mobility of load carriers, easier charge injection process and larger surface area.

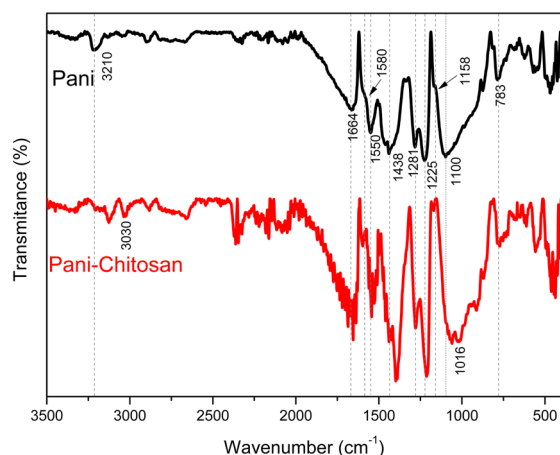


Figure 3. ATR-FTIR spectra of materials synthesized.

The thermogravimetric analysis of the Pani, Chitosan and Pani-Chitosan materials are shown in Figure 5. The thermogravimetric curve of chitosan presents two stages of mass loss: the first stage occurs between 20–200 °C with mass loss of 8.46% relative to water loss, while the second stage between 200–800 °C is relative to mass loss of 64.85% attributed to the decomposition of chitosan chains. The final residue was estimated around 26.40%.

Pani sample presented 3 stage of mass loss: the first stage occurs between 20–150°C with mass loss of 13.13% relative to water loss, HCl and volatile components; the second stage, between 150–400°C, with 6.08% of loss weight and is relative to release of oligomers and vaporization of dopant ions; the third and last stage, between 400–800°C, with 14.61% of loss weight, is relative to degradation of the polymer chains of Pani and rupture of the benzene rings; and finally, 66.34% of residue [44, 45].

Pani-Chitosan showed a very similar behavior compared to pure Pani sample, with lower loss weight until 330°C, indicating an improvement in the thermal stability of Pani. In temperatures exceeding 330°C, Pani-Chitosan presented higher lost weight than pure Pani, because in this temperature range, Chitosan chains start to

degrade and the final mass is equal to Pani. The increase of thermal stability in Pani-Chitosan can be attributed to the increase of the intra and inter hydrogen bonds in the polymer chain of Pani, by the presence of hydroxyl, amino and acetyl groups of Chitosan [46].

The electrochemical behavior of Pani is widely described in literature and two different processes can be described: the conversion from leucoemeraldine base to emeraldine salt and emeraldine salt to pernigraniline base. The position and shape of voltammetric peak changes according to the employed electrolyte and scan rate, because the charge compensation strongly depends on the proton diffusional process through in/out the polymer.

Figure 6 shows the cyclic voltammograms of materials obtained at the scan rate of 50 mVs⁻¹, however, similar results were obtained at 5, 10, 25, 75, 100, 125, 150, 250 and 500 mVs⁻¹. Both materials exhibit well-defined and reversible electroactivity. The two characteristic pairs of peaks of Pani at 0.24/0.03V and 0.87/0.83V are clear; the peak at 0.24V is higher due to high proton and anion current, while the reverse peak (0.03V) is less intense due to the lower mobility of the anions [47].

There are a pair of redox peaks in 0.4–0.6V region, which are assigned to Pani degradation, and the formation of cross-links between the chains and redox processes in oligomers produced in the synthesis [28, 40]. Pani-Chitosan presented current density higher than pure Pani, 3.12 times at 500 mVs⁻¹ for example, indicating that this material present a greater number of active sites available for the oxidation-reduction process.

The morphologies indicated by SEM images corroborate with cyclic voltammetry results, which are consistent with like a plate morphology of Pani-Chitosan sample, presenting a greater number of available active sites and a smaller ion diffusion path generating higher densities of current. On the other hand, pure Pani forms agglomerates, presenting a smaller active area, hindering the ionic diffusion through the material [38]. In addition, at high current densities, cyclic voltammetry curve of the Pani-Chitosan material exhibits a larger area among all materials, suggesting an excellent capacitance enhancement due to the interaction between Pani

and Chitosan [48].

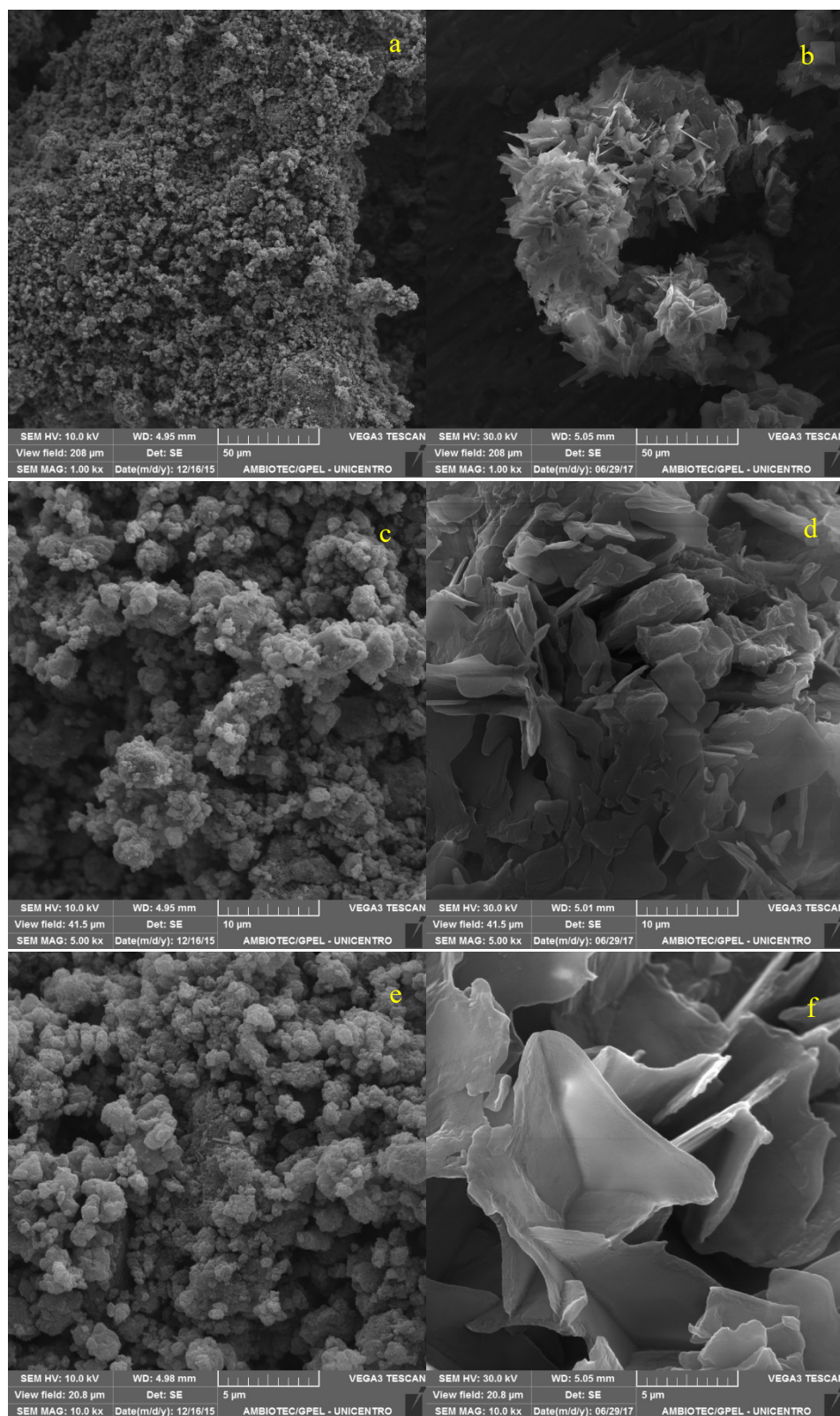


Figure 4. SEM images of Pani (a, c and e) and Pani-Chitosan (b, d and f) at 1kx (a and b), 5kx (c and d) and 10kx (e and f) of magnification.

The currents of the 0.24V peak obtained at scan rates of 5, 10, 25, 50, 75, 100, 125, 150, 250 and 500 mVs^{-1} of Pani and Pani-Chitosan are compared in Figure 7. Pani-Chitosan showed higher current than pure Pani in all scan rate studied. The difference is greater at higher scan rate, 3,12 times at 500 mVs^{-1} for example. These density current obtained are upper than those reported in literature to Pani and its composites, as Pani/ WO_3 [9], Pani/CNT [20], Pani/ MoS_2 [49], Pani/Cu (II) [22], Pani/Cu [45] and Pani/frGO [48].

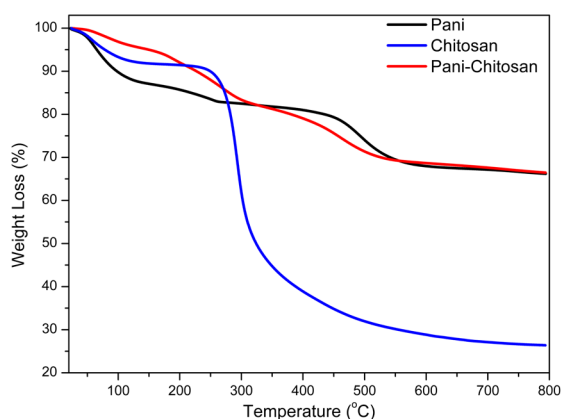


Figure 5. Thermogravimetric analysis of Pani, Chitosan and Pani-Chitosan from 20 to 800 °C, heating ramp to 10°C min^{-1} , at N_2 atmosphere.

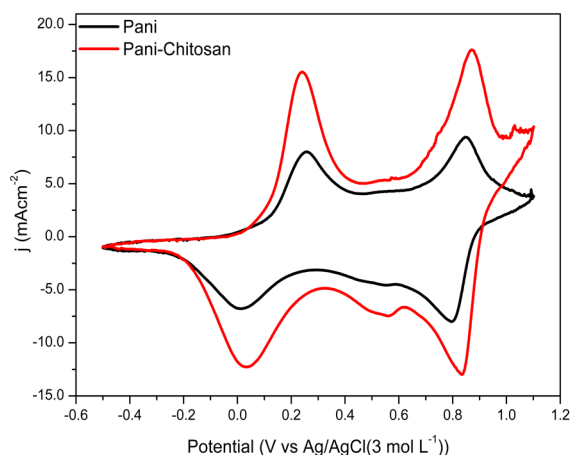


Figure 6. Cyclic voltammogram of Pani and Pani-Chitosan in H_2SO_4 (0.5 mol L^{-1}) at a scan rate of 50 mV s^{-1} .

In order to know the aspects related to the redox processes that occur in the studied materials, Figure 8 presents the cyclic voltammograms obtained from Pani and Pani-Chitosan at scan rate of 5, 10, 25, 50, 75, 100, 125, 150, 250 and 500 mVs^{-1} . The sharper and

shifted peaks in more negative potentials in Pani-Chitosan indicate that the charge injection process was facilitated, compared to pure Pani. The change of the peaks position at higher scan rates is stronger in Pani, indicating a faster charge compensation processes.

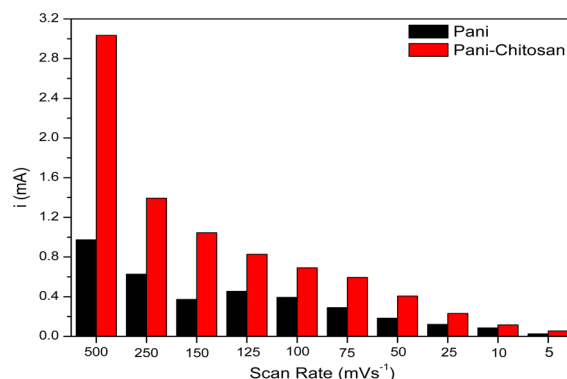


Figure 7. Current of peak in 0.24V for Pani and Pani-Chitosan at the scan rate studied.

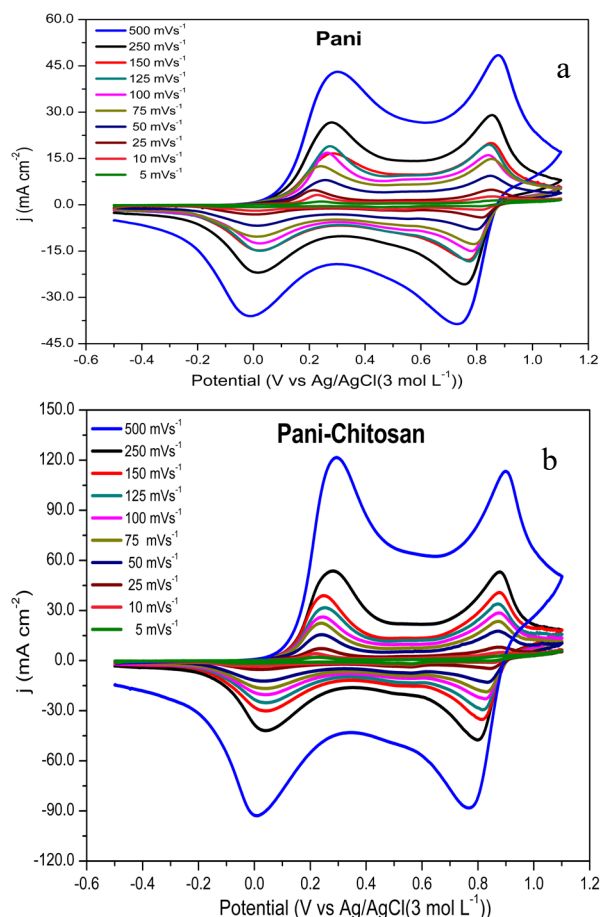


Figure 8. Voltammogram cyclic of Pani (a) and Pani-Chitosan in H_2SO_4 (0.5 mol L^{-1}) at scan rate of 5, 10, 25, 50, 75, 100, 125, 150, 250 and 500 mV s^{-1} .

4. Conclusions

In this study, a facile method for the synthesis of Pani-Chitosan plates with higher solubility was described. The composite synthesized was characterized by different analytical techniques such as UV-Vis, FTIR, SEM, TG and CV. FTIR and UV-Vis, which showed that hybrid material presents the characteristic bands of Pani in the emeraldine salt form, with small displacements to the region of greater energy, indicating an interaction of the polymer matrix of Pani with the chitosan chains. SEM images indicate that Pani presents morphology in the form of agglomerates, while Pani-Chitosan material presents fibrous morphology, indicating potential application in supercapacitors, due to its high surface area. The thermogravimetric analysis indicated that composite exhibit higher thermal stability than the pure Pani, which may be related to the interaction between the Pani and chitosan chains by means of van der Waals forces. The cyclic voltammograms show 2 pairs of characteristic Pani peaks. The hybrid material presented higher current densities at all studied scanning speeds and better defined peaks, indicating a greater number of accessible active sites and more facilitated loading injection processes. Morphologic, thermal and voltammetry characteristic of Pani-Chitosan indicate that the composite is a promising material for applications in electrochromic devices and capacitors, because of its greater surface area and electrochemical and thermal stability.

Acknowledgments

CNPq, CAPES, FINEP, LabGati, LabMat, Lapeci and Fundação Araucária, Rafael Marangoni for SEM images, Rodrigo de Carvalho Pereira for FTIR spectra and Patricia Oliveira for TG measurements.

References and Notes

- [1] Ćirić-Marjanović, G. *Synth. Met.* **2013**, *177*, 1. [\[Crossref\]](#)
- [2] Li, D.; Kaner, R. B. *J. Am. Chem. Soc.* **2006**, *128*, 968. [\[Crossref\]](#)
- [3] Zilberman, M.; Titelman, G. I.; Siegmann, A.; Haba, Y.; Narkis, M.; Alperstein, D. *J. Appl. Polym. Sci.* **1997**, *66*, 243. [\[Crossref\]](#)
- [4] Hu, N.; Zhang, L.; Yang, C.; Zhao, J.; Yang, Z.; Wei, H.; Liao, H.; Feng, Z.; Fisher, A.; Zhang, Y.; et al. *Sci. Rep.* **2016**, *6*, 19777. [\[Crossref\]](#)
- [5] Wang, X.; Shen, Y.; Xie, A.; Li, S.; Cai, Y.; Wang, Y.; Shu, H. *Biosens. Bioelectron.* **2011**, *26*, 3063. [\[Crossref\]](#)
- [6] Basak, S. P.; Kanjilal, B.; Sarkar, P.; Turner, A. P. F. *Synth. Met.* **2013**, *175*, 127. [\[Crossref\]](#)
- [7] Ashraf, P. M.; Lalitha, K. V.; Edwin, L. *Sensors Actuators, B Chem.* **2015**, *208*, 369. [\[Crossref\]](#)
- [8] Ayad, M. M.; Torad, N. L. *Sensors Actuators, B Chem.* **2010**, *147*, 481. [\[Crossref\]](#)
- [9] Hicks, S. M.; Killard, A. J. *Sensors Actuators, B Chem.* **2014**, *194*, 283. [\[Crossref\]](#)
- [10] Li, Z. F.; Blum, F. D.; Bertino, M. F.; Kim, C. S. *Sensors Actuators, B Chem.* **2012**, *161*, 390. [\[Crossref\]](#)
- [11] Steffens, C.; Manzoli, A.; Oliveira, J. E.; Leite, F. L.; Correa, D. S.; Herrmann, P. S. P. *Sensors Actuators, B Chem.* **2014**, *191*, 643. [\[Crossref\]](#)
- [12] Kulkarni, M. V.; Apte, S. K.; Naik, S. D.; Ambekar, J. D.; Kale, B. B. *Smart Mater. Struct.* **2012**, *21*, 35023. [\[Crossref\]](#)
- [13] Lu, H.; Zhou, Y.; Vongehr, S.; Hu, K.; Meng, X. *Synth. Met.* **2011**, *161*, 1368. [\[Crossref\]](#)
- [14] Grace, A. N.; Choi, S. Y.; Vinoba, M.; Bhagiyalakshmi, M.; Chu, D. H.; Yoon, Y.; Nam, S. C.; Jeong, S. K. *Appl. Energy* **2014**, *120*, 85. [\[Crossref\]](#)
- [15] Kumar, M.; Khan, M. A.; AlOthman, Z. a.; Siddiqui, M. R. *Desalination* **2013**, *325*, 95. [\[Crossref\]](#)
- [16] Ai, L.; Jiang, J. *Mater. Lett.* **2011**, *65*, 1215. [\[Crossref\]](#)
- [17] Jiang, F.; Li, W.; Zou, R.; Liu, Q.; Xu, K.; An, L.; Hu, J. *Nano Energy* **2014**, *7*, 72. [\[Crossref\]](#)
- [18] Hai, Z.; Gao, L.; Zhang, Q.; Xu, H.; Cui, D.; Zhang, Z.; Tsoukalas, D.; Tang, J.; Yan, S.; Xue, C. *Appl. Surf. Sci.* **2016**, *361*, 57. [\[Crossref\]](#)
- [19] Mu, J.; Ma, G.; Peng, H.; Li, J.; Sun, K.; Lei, Z. *J. Power Sources* **2013**, *242*, 797. [\[Crossref\]](#)
- [20] Bavio, M. A.; Acosta, G. G.; Kessler, T. *J. Power Sources* **2014**, *245*, 475. [\[Crossref\]](#)
- [21] Lin, W.; Xu, K.; Xin, M.; Peng, J.; Xing, Y.; Chen, M. *RSC Adv.* **2014**, *4*, 39508. [\[Crossref\]](#)
- [22] Pandey, K.; Yadav, P.; Mukhopadhyay, I. *J. Electroanal. Chem.* **2015**, *745*, 88. [\[Crossref\]](#)
- [23] Dalmolin, C.; Biaggio, S. R.; Rocha-Filho, R. C.; Bocchi, N. *Electrochim. Acta* **2009**, *55*, 227. [\[Crossref\]](#)
- [24] Mohan, V. M.; Chen, W.; Murakami, K. *Mater. Res. Bull.* **2013**, *48*, 603. [\[Crossref\]](#)
- [25] Wang, Y.; Li, B.; Zeng, L.; Cui, D.; Xiang, X.; Li, W. *Biosens. Bioelectron.* **2013**, *41*, 582. [\[Crossref\]](#)
- [26] Pandiyarajan, T.; Mangalaraja, R. V.; Karthikeyan, B. *Spectrochim. Acta - Part A Mol. Biomol. Spectrosc.* **2015**, *147*, 280. [\[Crossref\]](#)
- [27] Mohanraju, K.; Sreejith, V.; Ananth, R.; Cindrella, L. J. *J. Power Sources* **2015**, *284*, 383. [\[Crossref\]](#)
- [28] Janáky, C.; de Tacconi, N. R.; Chanmanee, W.; Rajeshwar, K. *J. Phys. Chem. C* **2012**, *116*, 4234. [\[Crossref\]](#)
- [29] Razak, S.; Nawil, M. A.; Haitham, K. *Appl. Surf. Sci.* **2014**, *319*, 90. [\[Crossref\]](#)

- [30] Yadav, S.; Devi, R.; Bhar, P.; Singhla, S.; Pundir, C. S. *Enzyme Microb. Technol.* **2012**, *50*, 247. [\[Crossref\]](#)
- [31] Thanpitcha, T.; Sirivat, A.; Jamieson, A. M.; Rujiravanit, R. *Carbohydr. Polym.* **2006**, *64*, 560. [\[Crossref\]](#)
- [32] Pandiselvi, K.; Thambidurai, S. *Mater. Sci. Semicond. Process.* **2015**, *31*, 573. [\[Crossref\]](#)
- [33] Kim, S. J.; Kim, M. S.; Kim, S. I.; Spinks, G. M.; Kim, B. C.; Wallace, G. G. *Chem. Mater.* **2006**, *18*, 5805. [\[Crossref\]](#)
- [34] Li, W.; Jang, D. M.; An, S. Y.; Kim, D.; Hong, S.-K. K.; Kim, H. *Sensors Actuators, B Chem.* **2011**, *160*, 1020. [\[Crossref\]](#) *Chem. Eng. J.* **2015**, *263*, 168. [\[Crossref\]](#)
- [36] Kannusamy, P.; Sivalingam, T. *Polym. Degrad. Stab.* **2013**, *98*, 988. [\[Crossref\]](#)
- [37] Castro, E. G. de; Zarbin, A. J. G.; Oliveira, H. P. de; Galembeck, A. *Synth. Met.* **2004**, *146*, 57. [\[Crossref\]](#)
- [38] Quintanilha, R. C.; Orth, E. S.; Grein-lankovski, A.; Riegel-Vidotti, I. C.; Vidotti, M. J. *Colloid Interface Sci.* **2014**, *434*, 18. [\[Crossref\]](#)
- [39] Wu, W.; Pan, D.; Li, Y.; Zhao, G.; Jing, L.; Chen, S. *Electrochim. Acta* **2015**, *152*, 126. [\[Crossref\]](#)
- [40] Oliveira, M. M.; Castro, E. G.; Canestraro, C. D.; Zanchet, D.; Ugarte, D.; Roman, L. S.; Zarbin, A. J. G. *J. Phys. Chem. B* **2006**, *110*, 17063. [\[Crossref\]](#)
- [41] Muthu Prabhu, S.; Meenakshi, S. *Int. J. Biol. Macromol.* **2016**, *85*, 16. [\[Crossref\]](#)
- [42] Yang, X.; Li, B.; Wang, H.; Hou, B. *Prog. Org. Coatings* **2010**, *69*, 267. [\[Crossref\]](#)
- [43] Mostafa, T. B.; Darwish, A. S. *Chem. Eng. J.* **2014**, *243*, 326. [\[Crossref\]](#)
- [44] Kannusamy, P.; Sivalingam, T. *Polym. Degrad. Stab.* **2013**, *98*, 988. [\[Crossref\]](#)
- [45] Divya, V.; Sangaranarayanan, M. V. *Eur. Polym. J.* **2012**, *48*, 560. [\[Crossref\]](#)
- [46] Cabuk, M.; Yavuz, M.; Unal, H. I. *Colloids Surfaces A Physicochem. Eng. Asp.* **2014**, *460*, 494. [\[Crossref\]](#)
- [47] Tawde, S.; Mukesh, D.; Yakhmi, J. V. *Synth. Met.* **2002**, *125*, 401. [\[Crossref\]](#)
- [48] Qiu, H.; Han, X.; Qiu, F.; Yang, J. *Appl. Surf. Sci.* **2016**, *376*, 261. [\[Crossref\]](#)
- [49] Huang, K.; Wang, L.; Liu, Y.-J.; Wang, H.-B.; Liu, Y.; Wang, L. *Electrochim. Acta* **2013**, *109*, 587. [\[Crossref\]](#)